Biosensors and Bioelectronics ■ (■■■■) ■■■–■■■

Contents lists available at ScienceDirect

Biosensors and Bioelectronics

journal homepage: www.elsevier.com/locate/bios

Fabrication of a novel dual mode cholesterol biosensor using titanium dioxide nanowire bridged 3D graphene nanostacks

S. Komathi [a,1], N. Muthuchamy [a,1], K-P. Lee [a,c], A-I. Gopalan [b,c,*]

[a] Deparment of Chemistry Education, Kyungpook National University, Daegu, South Korea
[b] Research Institute of Advanced Energy Technology, Kyungpook National University, Daegu, South Korea
[c] Department of Nanoscience and Nanotechnology, Kyungpook National University, Daegu, South Korea

ARTICLE INFO

Article history:
Received 14 September 2015
Received in revised form
6 November 2015
Accepted 14 November 2015

Keywords:
Nanostacks
Titanium dioxide
Graphene
Photoelectrochemical
Direct electron transfer
Cholesterol

ABSTRACT

Herein, we fabricated a novel electrochemical–photoelectrochemical (PEC) dual-mode cholesterol biosensor based on graphene (G) sheets interconnected-graphene embedded titanium nanowires (TiO_2(G)-NWs) 3D nanostacks (designated as G/Ti(G) 3DNS) by exploiting the beneficial characteristics of G and TiO_2-NWs to achieve good selectivity and high sensitivity for cholesterol detection. The G/Ti(G) 3DNS was fabricated by the reaction between functionalized G and TiO_2(G)-NWs. Cholesterol oxidase (ChOx) was subsequently immobilized in to G/Ti(G) 3DNS using chitosan (CS) as the binder and the dual mode G/Ti(G) 3DNS/CS/ChOx biosensor was fabricated. The electro-optical properties of the G/Ti(G) 3DNS/CS/ChOx bioelectrode were characterized by cyclic voltammetry and UV–vis diffuse reflection spectroscopy. The cyclic voltammetry of immobilized ChOx showed a pair of well-defined redox peaks indicating direct electron transfer (DET) of ChOx. The amperometric reduction peak current (at −0.05 V) linearly increased with increase in cholesterol concentration. The G/Ti(G) 3DNS/CS/ChOx bioelectrode was selective to cholesterol with a remarkable sensitivity (3.82 μA/cm^2 mM) and a lower detection limit (6 μM). Also, G/Ti(G) 3DNS/CS/ChOx functioned as photoelectrode and exhibited selective detection of cholesterol under a low bias voltage and light irradiation. Kinetic parameters, reproducibility, repeatability, storage stability and effect of temperature and pH were evaluated. We envisage that G/Ti(G) 3DNS with its prospective characteristics, would be a promising material for wide range of biosensing applications.

1. Introduction

Determination of cholesterol level in human blood is of great significance in clinical diagnostics (Sekretaryova et al., 2014). Electrochemical biosensors offer the advantages such as specific recognition of cholesterol, low cost and rapid quantification (USA Pat. no: 53405339). Electrochemical cholesterol biosensors were generally fabricated through immobilization of an enzyme, such as cholesterol oxidase (ChOx) or cholesterol esterase (ChEt), onto a suitable substrate (Tan et al., 2005; Chong et al., 2002). A review that highlights the materials and techniques utilized for the design and construction of cholesterol biosensor has been published (Arya et al., 2008). Various enzyme immobilization matrices based on graphene (G), chitosan (CS), titanium dioxide (TiO_2), conducting polymers (CPs), carbon nanotube and their nanocomposites (NCs) were developed/used for the construction of electrochemical cholesterol biosensors (Supporting Information(SI)-1). The establishment of direct electron transfer (DET) between the redox enzyme and electrode has been utilized for the development of third generation biosensors (Manesh et al., 2010; Komathi et al., 2013). The DET based biosensors can be operated at a lower potential and hence electrochemical interferences by many of the co-existing species are easily avoided. Carbon nanomaterials, such as G and carbon nanotubes, have been widely utilized in the study for direct electrochemistry of enzymes (Sheng et al., 2014; Ueda et al., 2011). Unfortunately, the DET between the cholesterol sensing enzyme (ChOx or ChEt) and the electrode could not be achieved with many of the matrices (Manjunatha et al., 2011; Sharma et al., 2015). The two main problems; (i) poor electronic communication between the active site of an enzyme and the electrode and (ii) leaching of the enzyme from the electrode surface (Unnikrishnan et al., 2013), restricted the development of DET based cholesterol sensors.

Recently, photoelectrochemical (PEC) biosensors have been projected as the alternative to conventional electrochemical or optical sensors due to their high sensitivity (Devadoss et al., 2015).

* Corresponding author at: Research Institute of Advanced Energy Technology, Kyungpook National University, Daegu, South Korea.
E-mail address: algopal_99@yahoo.com (A.-I. Gopalan).
[1] Authors contributed equally to this work.

http://dx.doi.org/10.1016/j.bios.2015.11.042
0956-5663/

In a typical PEC based biosensor, an analyte (or biomolecule) can influence the photocurrent through oxidation or reduction process, and such the photocurrents can be correlated to the quantity of an analyte. Generally, the photophysical properties of semiconductor metal oxides such as TiO_2 are exploited towards developing PEC biosensors (Hu et al., 2013). PEC sensors involve sequence of charge transfer processes between the analyte and photocatalytic material/electrode, before harvesting the generated photocurrent. To enhance the generated photocurrent of at semiconductor electrode, the separation of hole (h^+)-electron species is required. However, effective separation of h^+-electron pairs is a challenge for the PEC based biosensors. Alternatively, the suppression of photocurrents by an analyte or sensitizer opens up a new avenue for the fabrication of PEC devices and sensors (Zang et al., 2014; Han et al., 2015b; Li et al., 2015a).

The effective shuttling of electron to the electrode surface or analyte is vital and deciding factor for quantifying the analyte detection in a PEC. The photoactive material can be structurally modified to augment DET between the redox enzyme and electrode. Thus, it is envisaged that the fabrication of a biosensor with excellent performances, in both PEC and electrochemical modes, requires manipulation of electron capture and transport properties of the semiconducting material. Also, a PEC fabricated with an additional DET feature for the immobilized enzyme, can have the unique advantage of detecting an analyte at a lower applied potential through the electrochemical sensing. However, studies on DET based PEC biosensors are scarce. In this work, we designed to fabricate a novel electrochemical-PEC dual mode biosensor using the combination of G embedded TiO_2 nanostacks (NS) as the photoactive material and CS as the polymer support to providing biocompatible microenvironment for the immobilized enzyme. Importantly, the designed hybrid nanoarchitecture, namely NS, provides DET for the immobilized enzyme and supports the generation of photocurrents.

It is known that hierarchically ordered nanostructures, such as nanowires (NWs) (Zhuang et al., 2008) and nanoflowers (Sai-Anand et al., 2013), have been demonstrated to show significantly enhanced electron transport and excellent electrochemical properties. Recently, nucleation and growth of graphitic carbon or metal–organic frameworks facilitated the generation of NS, and opened across a wide range of applications (Van Gough et al., 2014). As compared with bulk materials, TiO_2 nanostructures have the advantages of a large specific surface area and a high surface adsorption that are beneficial for photocatalytic applications (Chen et al., 2012). One dimensional (1D) TiO_2 nanostructures play an important role in PEC measurements due to their fast electron transport properties and a higher diffusion of redox species (Stafiniak et al., 2011). Doping of TiO_2 with G sheets improved the photocatalytic performances, in-terms of extended light absorption and decreased rate of recombination of photogenerated h^+-electron pairs (Lee et al., 2012). CS exhibits good chelating ability and has high content of amino (–NH) and hydroxyl (–OH) groups. With these features, CS has been utilized as a biopolymer for the immobilization of a desired enzyme (Suginta et al., 2013). To the best of our knowledge, the preparation of hierarchically ordered G embedded TiO_2-NWs (TiO_2(G)-NWs) in the form of NS and fabrication of electrochemical-PEC dual mode biosensor are new aspects and have not been reported so far.

In this work, we reported the fabrication of a novel electrochemical-PEC dual mode biosensor utilizing the beneficial components such as G, TiO_2(G)-NWs and CS and transforming them into a NS through establishment of chemical interactions between modified TiO_2-NWs and G. We designated the assemblies of G and TiO_2(G)-NWs as G/Ti(G)-3DNS. The G/Ti(G)-3DNS was further modified with CS and used for immobilization of ChOx to fabricate the biosensor G/Ti(G)-3DNS/CS/ChOx and used as the

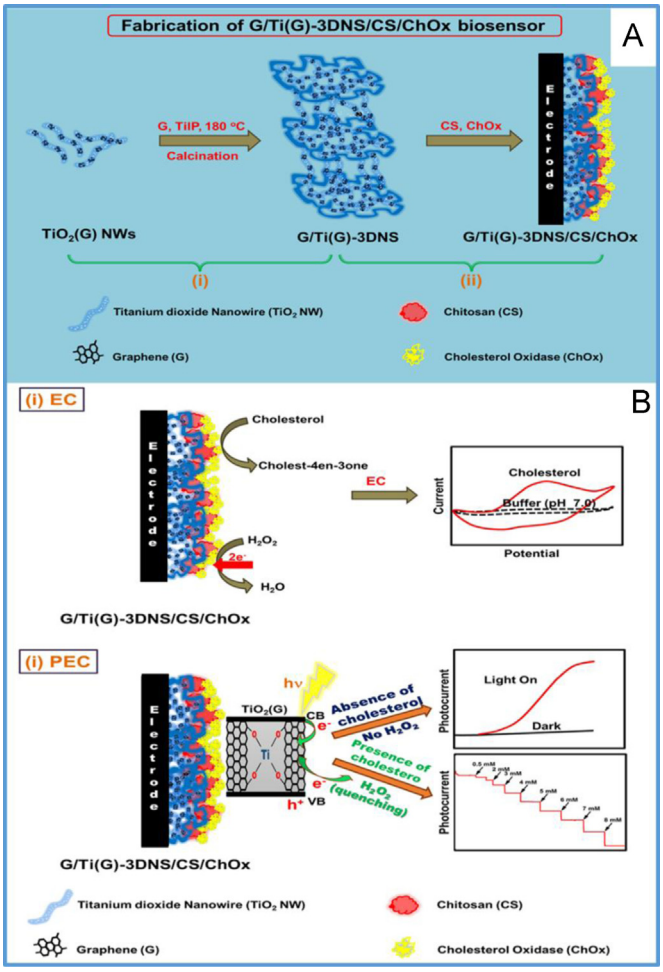

Scheme 1. (A) Stages in the fabrication of electrochemical–photoelectrochemical dual mode biosensor using G/Ti(G)-3DNS/CS/ChOx. Stage (i); Transformation of TiO_2(G)-NWs to G/Ti(G)-3DNS Stage (ii); modification of G/Ti(G)-3DNS with CS and immobilization of CS. (B) The electrochemical (i) and photoelectrochemical (ii) sensing of cholesterol at G/Ti(G)-3DNS/CS/ChOx biosensor. (i) Cyclic voltammogram showing increased current in the presence of cholesterol and (ii) Photocurrent generation in the presence of light irradiation at G/Ti(G)-3DNS/CS/ChOx biosensor and variations of amperometric photocurrents for the changes in the concentrations of cholesterol.

electrochemical-PEC dual mode biosensor for the detection of cholesterol. To ensure the electrochemical connectivity in the 3DNS architecture, TiO_2-NWs were first embedded with G and used as TiO_2(G)-NWs. Further, the photoactive G/Ti(G)-3DNS was prepared. The brief description on the making of G/Ti(G)-3DNS is as follows. Initially, TiO_2(G)-NWs were prepared as reported earlier (Lee et al., 2015a) and subsequently transformed into G/Ti(G)-3DNS by the reactions of carboxyl functionalized G sheets (G–COOH) with titanium isopropoxide (TiIP) via a modified hydrothermal method (Liu and Aydil 2009; Han et al., 2015a). The G/Ti(G)-3DNS were produced through assembling of the 1D TiO_2(G)-NWs as the pillars for the 2D G sheets through titanate coating onto TiO_2(G)-NWs (Scheme 1(A)). The –COOH groups in G–COOH participated in the hydrolysis and condensation processes with TiIP and formed the channels for the interconnection between TiO_2 coated TiO_2(G)-NWs and G sheets (Scheme 1(A)). The G/Ti(G)-3DNS was used as an electrode modifier on the surface of indium tin oxide (ITO) coated glass or glassy carbon (GC) electrode and subsequently immobilized with ChOx using CS as the binder (Scheme 1(A)). The fabricated G/Ti(G)-3DNS/CS/ChOx biosensors was utilized for the detection of cholesterol in electrochemical-PEC (dual) modes (Scheme 1(B)). The Ti(G)-3DNS/CS/ChOx

exhibited good direct electrochemistry for ChOx, which is beneficially utilized for the fabrication of mediator free electrochemical sensor to detect cholesterol at a lower potential with a good selectivity. On the other hand, the PEC results indicated that Ti(G)-3DNS/CS/ChOx exhibited a larger photocurrents than TiO_2-NWs and TiO_2(G)-NWs electrodes and showed linear variation in the photocurrent for cholesterol concentration.

2. Experimental

2.1. Chemicals

The chemicals, Ti(IV) isopropoxide (97%) (TiIP), chitosan (CS, ≥75% deacetylated) derived from shrimp shells (Pandalus borealis), choesterol oxidase (ChOx), Triton™ X-100, Nafion and acetic acid were obtained from Sigma-Aldrich, S. Korea. Human serum (from human male AB plasma, USA origin, sterile-filtered) was obtained from Sigma Aldrich (Korea). G nanoplatelet sheets were obtained from E NanoTEC (Korea). Polyvinylpyrrolidone (PVP, molecular weight <40,000, Fluka), ethanol (OCI, Korea), dimethyl formamide (OCI, Korea), isopropyl alcohol (OCI, Korea) and all other reagents were used as received. Phosphate buffer solution (PBS) (0.1 M, pH 7.0) was obtained from Dukson (Korea) chemicals. A stock solution of cholesterol was prepared in 10% (w/v) of Triton X-100+Isopropyl alcohol and 0.1 M PBS and then stored at 4 °C. A stock solution of ChOx was freshly prepared in 0.1 M PBS (Ruecha et al., 2011).

2.2. Preparation of G/Ti(g)-3DNS

Initially, TiO_2(G)-NWs were prepared by electrospinning a composite dope solution comprised of TiIP and G–COOH (SI-2) (Lee et al., 2015a). Similarly, pristine TiO_2-NWs were prepared through an electrospinning solution without having G-COOH in the dope. About 10 mg of G–COOH were dispersed in water–DMF mixture solution (1:7) and sonicated for about 20 min (Branson digital sonifier). To this dispersant, 40 mg of TiO_2(G)-NWs were added and magnetically stirred for 2 h at 80 °C. Then, 0.23 mL TiIP was added and the resulting suspension was further stirred for 6 h at 80 °C. The resulting composite (G–COOH, TiO_2(G)-NWs, TiIP) suspension was transferred in to a cylindrical vial containing 10 mL distilled water and heated in an oven at 180 °C for 12 h. Finally, the as prepared sample (G/Ti(G)-3DNS) was washed with ethanol and dried for 2 h. Similarly, control experiments were also carried out for the preparation of G/Ti-3DNS using pristine TiO_2-NWs.

2.3. Fabrication of G/Ti(G)-3DNS/CS/ChOx biosensor

A slurry was prepared by dispersing 5 mg of G/Ti(G)-3DNS in 1.2 mL of isopropyl alcohol–Nafion mixture (3:1) and sonicated. About 2 μL of the above dispersant was placed on the GC electrode or 7 μL on the surface of pre-cleaned ITO electrode and dried at 40 °C. ChOx was immobilized onto G/Ti(G)–3DNS using CS as the binder. At the first instant, 2 μL of CS (1 mg of CS in 2% acetic acid) was dropped over the G/Ti(G)–3DNS film and was allowed to dry. Then, about 6 μL of ChOx was dropped onto the surface of CS coated G/Ti(G)–3DNS film electrode and was again allowed to dry further for about 3 h to obtain G/Ti(G)–3DNS/CS/ChOx biosensor. The biosensor was stored at 4 °C in 0.1 M PBS and used for further experiments. Similarly, for comparative purposes, the other biosensors, G/Ti-3DNS/CS/ChOx, TiO_2/CS/ChOx and G/CS/ChOx, were fabricated.

2.4. Characterization

The morphology and composition of G/Ti(G)–3DNS was examined by field-emission scanning electron microscopy (FE-SEM, S-4300 & EDX-350, Hitachi, Japan) and transmission electron microscopy (TEM, HD-2300, Hitachi, Japan, 200 kV). The optical properties of G/Ti(G)-3DNS/CS/ChOx were characterized by a UV–vis diffuse reflectance UV/vis/NIR spectrometer (Cary 5000, Agilent, Korea). All electrochemical experiments were carried out using Iviumstat and Compactstat (The Netherlands).

2.4.1. Electrochemical experiments

Typically, a conventional three electrode cell set-up, comprising of GCE modified G/Ti(G)-3DNS/CS/ChOx (working), a platinum wire (counter), and a Ag/AgCl (reference) electrode was used for the electrochemical measurements. Electrochemical impedance spectroscopy (EIS) measurements were performed in a solution of 5 mM $K_3Fe(CN)_6/K_4Fe(CN)_6$ (1:1) (0.1 M KCl) within the frequency range of 10 mHz to 100 kHz.

2.4.2. Cholesterol sensing by PEC and electrochemical modes

For PEC biosensor measurements, ITO was modified with G/Ti (G)–3DNS/CS/ChOx to fabricate the biosensors. The PEC measurements were carried out by irradiation with a lamp (Viller Lourmat, France, 365 nm (4 W) placed at a distance of 10 cm from the working electrode surface. The cholesterol sensor measurements were done by immersing the ITO/G/Ti(G)–3DNS/CS/ChOx biosensor in 0.1 M PBS (pH=7.0) solution containing different concentrations of cholesterol in an electrochemical cell. To confirm the feasibility of the fabricated G/Ti(G)-3DNS/CS/ChOx biosensor for real sample analysis, the amount of cholesterol in human blood serum samples (Human Serum (from human male AB plasma, USA origin, sterile-filtered), Sigma) was determined. Specifically, three human blood serum samples were prepared by adding different concentrations (2, 4, and 6 mM) of standard cholesterol solution (0.1 M PBS; pH=7.0). The recovery of cholesterol concentration were determined. Amperometry was applied as the measuring technique for both PEC, electrochemical and real sample cholesterol detection.

3. Results and discussion

3.1. Morphology and optical properties

The precursors, TiO_2(G) NWs and G–COOH, were transformed in to G/Ti(G)-3DNS via hydrolysis of TiIP and thermal treatment. During the heat treatment, hydrolysis and condensation of TiIP occurred on the surface of the TiO_2(G)–NWs. Also, the G–COOH, included in the titanate forming mixture participated in the sol–gel reactions. Considering these aspects, we presumed that TiO_2(G)–NWs were coated with a shell layer of titanate (TiO_2) and stacked with 2D G sheets during the heat treatment process. In brief, the participation of both 2D G sheets and 1D TiO_2(G)–NWs in the sol–gel reaction caused the transformation of TiO_2(G)–NWs to G/Ti(G)–3DNS.

FESEM image of G/Ti(G)–3DNS (Fig. 1A) shows a 3D stack type morphology, generated by the pillared 1D nanorods (titanate coated TiO_2(G)–NWs) of diameters in the range from 300 to 500 nm and the 2D G sheets. The initially prepared TiO_2(G)–NWs were found to have a smooth NW morphology with diameters around ~250 nm and G sheets embedded within NWs (Lee et al., 2015a, 2015b). The NWs were completely modified into nanorods, possibly during the heat treatment in the presence of TiIP and G–COOH. As a consequence, the diameters of NWs were increased to around 400–600 nm than the starting material, TiO_2(G)–NWs.

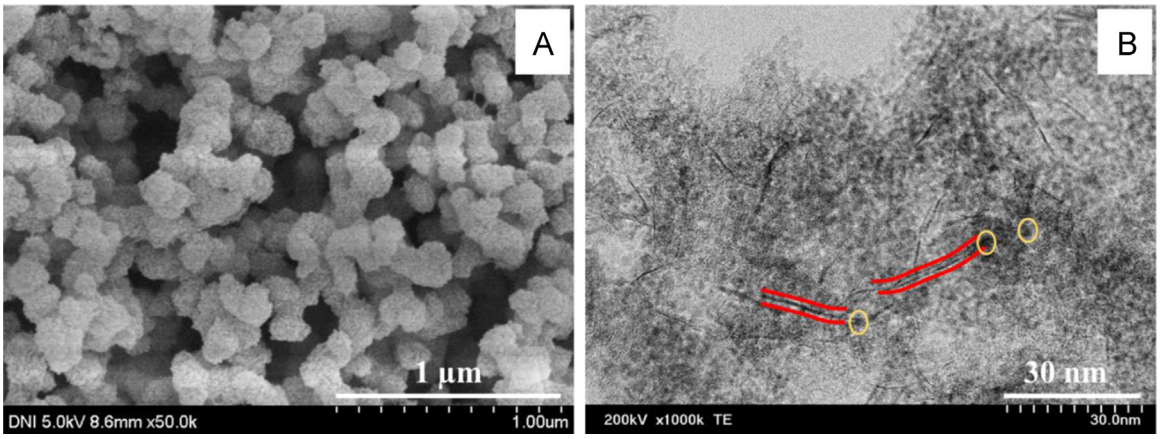

Fig. 1. FESEM images of (A) G/Ti(G)–3DNS. Low magnification HRTEM image (B) of TiO_2 NWs (red marking, vertical bar) and G (yellow marking, circle)

HRTEM image of G/Ti(G)–3DNS (Fig. 1B) shows the existence of building units, TiO_2 NWs (red marking) and G (yellow marking) (Fig. 1B).

It has been earlier reported that inclusion of G into semiconductor metal oxides influenced the optical properties (Rathi et al., 2015). The UV–vis DRS (SI-3 and SI-4) data were used to understand optical property changes due to the transformation of TiO_2(G)–NWs to G/Ti(G)–3DNS. Fig. SI-3 showed broad absorption peaks in the visible region for both G/Ti(G)–3DNS and G/Ti-3DNS in contrast to pristine TiO_2–NWs. The significant red shifting to the visible region for G/Ti(G)–3DNS as compared to TiO_2(G)–NW is possibly attributed to the formation of Ti–O–C bonds during the hydrothermal treatment (Xiang et al., 2011). In order to know the extent of optical property changes, the plots $(F(R_\alpha)h\upsilon)^2$ vs $h\upsilon$ (SI-4) were drawn using Kubelka–Munk equation (where $F(R_\alpha)$ is Kubelka–Munk function and R_α is the diffuse reflectance). The optical band gap (E_g) values were deduced by extending the straight line range of these plots to the $h\upsilon$ axis (Wu et al., 2013; Ma et al., 2010). As compared to the E_g value of TiO_2-NWs (3.2 eV), the E_g values of G/Ti-3DNS and G/Ti(G)–3DNS were 2.2 eV and 1.9 eV, respectively indicating modification in the optical properties (Chen et al., 2013).

3.2. Electrochemical performance of modified electrodes

Among the common bench mark redox system, $Fe(CN)_6^{3-/4-}$ redox probe was selected because it can exhibit excellent surface sensitive electrochemical responses toward modified electrodes. Cyclic voltammograms (CVs) of the different GCE modified electrodes (SI-5), G/Ti(G)–3DNS/CS/ChOx, G/Ti-3DNS/CS/ChOx, TiO_2/CS/ChOx and G/CS/ChOx, were recorded in the presence of 5 mM $Fe(CN)_6^{3-/4-}$ (each) in 0.1 M KCl to understand the electron transfer properties and effective surface area (A) of the modified electrodes. CVs of the bare and modified electrodes showed well-defined redox peaks corresponding to the reversible reaction of Fe $(CN)_6^{3-/4-}$ redox processes. The electron transport capability at the modified electrodes was compared using anodic or cathodic peak currents (I_{pa} or I_{pc}) of the $Fe(CN)_6^{3-/4-}$ redox transitions. The I_{pa} of G/Ti(G)–3DNS/CS/ChOx was ~1.96 and ~58.2 times higher than at the G/Ti-3DNS/CS/ChOx and TiO_2/CS/ChOx electrode. The electrodes modified with G incorporated materials, G/Ti(G)–3DNS/CS/ChOx and G/Ti-3DNS/CS/ChOx showed comparatively higher I_{pa} values than at the TiO2/CS/ChOx electrode. The results demonstrated that the presence of G sheets (both as interconnected and embedded form) in 3DNS nanoarchitectures augmented the electron transport capabilities of the modified electrodes as reported elsewhere (Ruecha et al., 2014). The electrochemical properties of G/CS/ChOx are also detailed in (SI-5).

CVs were recorded at G/Ti(G)-3DNS/CS/ChOx, G/Ti-3DNS/CS/ChOx and TiO_2/CS/ChOx (SI-6) in 5 mM $Fe(CN)_6^{3-/4-}$ (0.1 M KCl) solution for different scan rates (υ). Both anodic and cathodic peak currents were linear with square root υ, which demonstrated that the $Fe(CN)_6^{3-/4-}$ redox reaction was a diffusion controlled process at these electrodes (Gholivand and Khodadadian et al. 2014). For the reversible process and under diffusion conditions, the A of the modified electrodes was estimated according to the Randles–Sevcik equation (Siswana et al., 2006).

$$I_p = 2.69 \times 10^5 A D^{1/2} n^{3/2} \upsilon^{1/2} C \quad (1)$$

where I_p is the redox peak current, n is the number of electrons transferred ($n=1$) and D is diffusion coefficient ($D=0.76\times10^{-5}$ cm^2s^{-1} at 25 °C). The value of A for the G/Ti(G)-3DNS/CS/ChOx was about ~1.87 and ~6.23 times higher than the A of G/Ti-3DNS/CS/ChOx and TiO2/CS/ChOx, respectively. The results revealed that G/Ti(G)-3DNS/CS/ChOx possess the highest A as compared to rest of the modified electrodes.

The electron transfer behavior of the pristine TiO_2(G)–NWs and modified electrodes G/Ti-3DNS and G/Ti(G)-3DNS were studied by EIS. SI-7 shows the Nyquist plots of the modified electrodes. The semicircle diameter of the plots corresponds to the electron transfer resistance (R_{et}), which controls the electron transfer kinetics of the redox probe at the electrode interface. The R_{et} of pristine TiO_2(G)–NWs was 802 Ω. The R_{et} of G/Ti(G)-3DNS (730 Ω) electrode was lesser as compared TiO_2(G)–NWs (802 Ω). This can be attributed to the enhanced electron transfer behaviour of G/Ti(G)-3DNS as compared to TiO_2(G)–NWs. To know the influence of G, the R_{et} of G/Ti-3DNS was utilized. The R_{et} of G/Ti-3DNS (925 Ω) was much larger than the R_{et} of G/Ti(G)-3DNS (730 Ω). This infers that the G embedded within TiO_2 augmented the electron transfer kinetics. Upon further modification with CS and immobilization with ChOx, the values of R_{et} increased as; G/Ti(G)-3DNS/CS/ChOx (1720 Ω), G/Ti-3DNS/CS/ChOx (1870 Ω), TiO_2/CS/ChOx (2050 Ω), G/CS/ChOx (2620 Ω). The increase in R_{et} upon modification with CS and ChOx immobilization is due to the generation of the insulating polymer (CS) and protein (ChOx) layers on the assembled surface.

3.3. Direct electrochemistry of ChOx on G/Ti(G)-3DNS/CS/ChOx

To investigate the application of the G/Ti(G)-3DNS/CS/ChOx toward biosensing devices, the DET between ChOx on the G/Ti(G)-3DNS/CS/ChOx (Fig. 2(a)) was investigated in nitrogen saturated (oxygen free) 0.1 M PBS at 20 mVs^{-1} (Fig. 2(a)). The G/Ti(G)-3DNS/

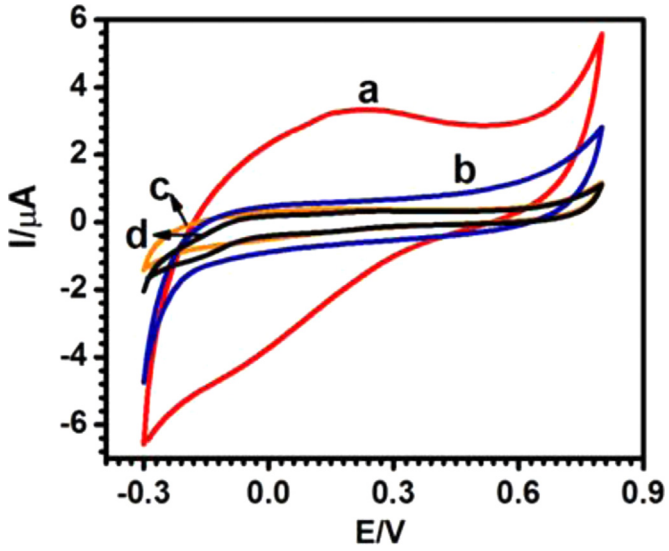

Fig. 2. Cyclic voltamograms of G/Ti(G)-3DNS/CS/ChOx (a), G/Ti-3DNS/CS/ChOx (b), TiO_2/CS/ChOx (c), G/CS/ChOx (d) in 0.1 M PBS (pH 7.0) at the scan rate of 20 mVs^{-1}.

CS/ChOx electrode shows a pair of well-defined redox peaks at +0.2/−0.02 V (versus Ag/AgCl) that corresponds to the DET reactions of the FAD/$FADH_2$ electroactive center in ChOx (Manjunatha et al., 2012; Cai and Chen, 2004). However, the other electrodes, G/Ti-3DNS/CS/ChOx (Fig. 2(b)), TiO_2/CS/ChOx (Fig. 2(c)) and G/CS/ChOx (Fig. 2(d)) electrodes did not show any obvious response for ChOx, indicating that the presence of both ChOx and G/Ti-3DNS/CS/ChOx on the electrode surface is necessary to achieve the DET of ChOx. The increased electrochemical signals of ChOx on G/Ti(G)-3DNS electrode might be attributed to two factors. Firstly, the biocompatible environment and 3D platform of G/Ti(G)-3DNS/CS provide necessary special orientation for ChOx molecules to retain their native enzyme activities. Secondly, G/Ti(G)-3DNS/CS (SI-8) possesses larger A to accommodate higher loading of ChOx. The effect of υ on the DET of ChOx at G/Ti(G)-3DNS/CS/ChOx was also investigated (SI-8). The results (SI-8) indicated that DET of ChOx on G/Ti(G)-3DNS/CS/ChOx is a surface-confined electron transfer process (Bard and Faulkner, 2001). The electrokinetic parameters were evaluated (SI-8). The electron transfer rate constant (k_s) value of G/Ti(G)-3DNS/CS/ChOx is higher than the apparent heterogeneous electron transfer rate constant value reported for ChOx at G/graphite electrode (0.78 s^{-1}) (Manjunatha et al., 2012) and Ag NPs/GSH/PDATA (0.75 s^{-1}) (Lin et al., 2011).

3.4. G/Ti(G)-3DNS/CS/ChOx as electrochemical biosensor for cholesterol (in oxygen free solution)

The DET based bioelectrocatalysis of ChOx towards cholesterol was investigated without (dashed line) and with 2 mM cholesterol (solid line) in an oxygen free 0.1 M PBS (pH 7.0) solution at G/Ti(G)-3DNS/CS/ChOx (Fig. 3A), G/Ti-3DNS/CS/ChOx (Fig. 3B), TiO2/CS/ChOx (Fig. 3C) and G/CS/ChOx (Fig. 3D), electrodes. The I_{pa} and I_{pc} significantly increased in the presence of cholesterol, which conformed the DET based bioelectrocatalysis for cholesterol. ChOx is characterized by its electroactive enzyme co-factor ChOx (FAD), which can be transformed to $FADH_2$ via two electron coupled with two proton redox reactions.

$$ChOx(FAD)+2H^+ +2e^- \rightarrow ChOx(FADH_2) \quad (2)$$

In the presence of cholesterol, ChOx (FAD) oxidizes cholesterol to cholest-4-en-3-one and transforms into ChOx($FADH_2$) (Eq. (3)) (Li et al., 2015b; Zhu et al., 2013). The ChOx ($FADH_2$) is oxidized back to

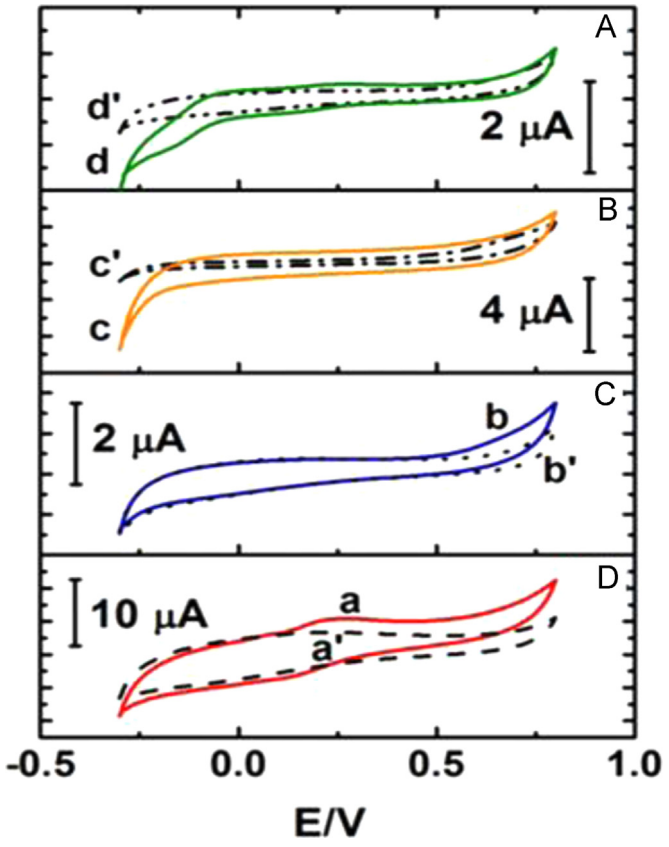

Fig. 3. Cyclic voltamograms of G/Ti(G)-3DNS/CS/ChOx (A), G/Ti-3DNS/CS/ChOx (B), TiO_2/CS/ChOx (C), G/CS/ChOx (D) (a,b,c an d d) in the presence of 0.5 mM cholesterol (pH 7.0) at the scan rate of 20 mVs^{-1}; (a',b',c' and d') in the absence of cholesterol solution.

ChOx (FAD) (Eq. (4)) and results in the restoration of ChOx (FAD) at the electrode surface without the role of any mediator. The process is termed as DET based bioelectrocatalysis of ChOx towards cholesterol. The DET bioelectrocatalysis can be described as

$$ChOx(FAD) + Chlesterol \rightarrow ChOx(FADH_2) + Cholest{-}4{-}en{-}3one \quad (3)$$

$$ChOx(FADH_2) \rightarrow ChOx(FAD) + 2H^+ + 2e^- \quad (4)$$

The electrochemical performance of the electrode is highly dependent on various factors that include specific surface area, electroconductivity and catalytic activity. Graphene included in the composite improves the conductivity (SI-7). We compared the electrochemical performance between graphene included and graphene excluded composites based electrodes. However a non-Faradaic increase in capacitance current was observed at the other electrodes, G/Ti-3DNS/CS/ChOx (Fig. 3B), TiO_2/CS/ChOx (Fig. 3C) and G/CS/ChOx (Fig. 3D) in the presence of cholesterol. The non-Faradaic current response at the graphene excluded composites based electrodes may be due to the absence of DET for ChOx as well the lesser conductive surfaces.

CVs of G/Ti-3DNS/CS/ChOx in 0.1 M PBS (SI-9) solution were also recorded for different concentrations of cholesterol. A linear increase in peak current was noticed for the increasing concentration of cholesterol.

3.5. Optimization of parameters for G/Ti(G)-3DNS/CS/ChOx as biosensor

Experimental conditions for the cholesterol biosensing were

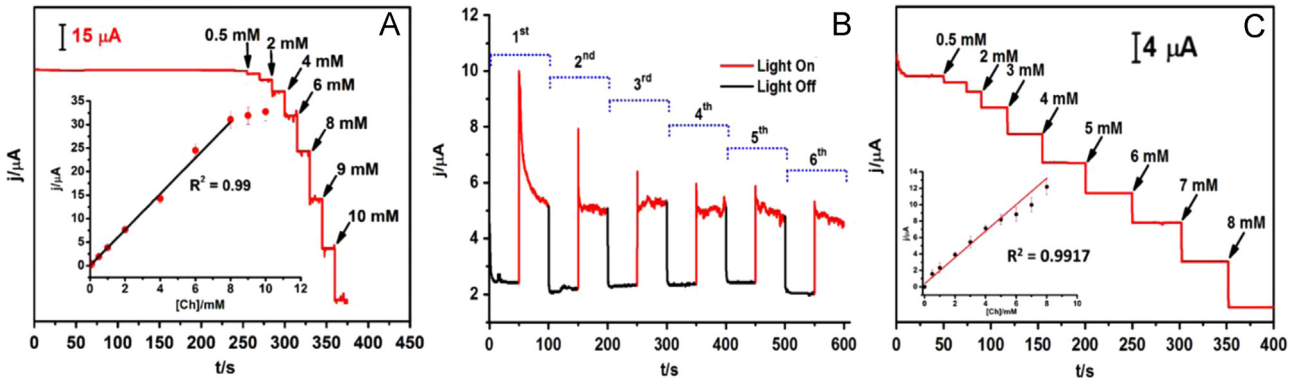

Fig. 4. (A) Amperometric response of G/Ti(G)-3DNS/CS/ChOx at −0.05 V upon successive addition of Cholesterol solution (pH 7.0) (Inset: linear calibration plot of concentration of cholesterol vs peak current). (B) Photoelectrochemical "on–off" amperometric response (light irradiation = 254 nm) of G/Ti(G)-3DNS/CS/ChOx in the presence of 2 mM cholesterol (pH 7.0) at −0.05 V. (C) Upon successive addition of cholesterol solution (pH 7.0) in "On state" (Inset: linear calibration plot of concentration of cholesterol vs peak current).

optimized in terms of pH, temperature and the amount of ChOx immobilized onto G/Ti(G)-3DNS/CS/ChOx and the details are presented in SI-10–12.

3.6. *Electrochemical sensing of cholesterol at G/Ti(G)-3DNS/CS/ChOx biosensor (in oxygen free solution)*

The amperometry experiments were performed at a potential of −0.05 V in N_2 saturated conditions. It was worthnoing that current due to the reduction of residual oxygen (if any) and its product (H_2O_2) did not overlap with currents at −0.05 V. This is due to the fact that oxygen reduction occurs around −0.015 V. Hence, the current (*i*)–time (*t*) transients witnessed for the successive addition of cholesterol is mainly due to DET bioelectrocatalysis of ChOx (Eqs. (3, and 4)). A typical *i*–*t* plot for successive step changes of cholesterol concentration on G/Ti(G)-3DNS/CS/ChOx is presented (Fig. 4A). The biosensor achieved 98% of steady state current within 2 s, which was recognized as the response time for cholesterol sensing. The response time is shorter than reported by many other biosensors such as ChOX in sol–gel film (51 s) (Yao and Takashima, 1998), MWNT(SH)–Au/Chi–IL/ChOx (7 s) (Gopalan et al., 2009), ChEt/ChOX/FG/Gr (3 s) (Manjunatha et al., 2012). Such a fast response is attributed to the stable immobilization of the cholesterol into G/Ti-3DNS/CS/ChOx and a faster DET at the electrode. Upon increasing the concentration of cholesterol, the response current steadily increased and reached the constancy at higher concentrations of cholesterol. The results suggested that the active sites of the enzyme may be saturated at higher cholesterol levels. The calibration plot, concentration of cholesterol vs current, is shown in Fig. 4A (inset). The G/Ti(G)-3DNS/CS/ChOx biosensor exhibited a linear concentration range for cholesterol from 50 μM to 8000 μM with an excellent correlation coefficient of $R^2 = 0.99$. The linear concentration range for cholesterol detection is much wider than other biosensors fabricated with different ChOx immobilization matrices (Table 1). The sensitivity of the cholesterol biosensor was 3.82 μA/ mM cm^2, which is much higher than that of other cholesterol biosensors (Table 1). The limit of detection (LOD) of the sensor is the lowest analyte concentrate that can be reliably distinguished from the blank solution (absence of an analyte) in with a stated level of confidence (~1%). Several conceptual approaches for reporting the LOD are available. One of the approaches involves the use of signal (*S*) to noise (*N*) ratio. The *S*/*N* ratio is the ratio of peak height for a given analyte concentration to the height of the blank signal (base line noise). A *S*/*N* ratio of 3 is generally considered acceptable for estimating LOD (Zhu et al., 2013; Li et al., 2015b; Tong et al., 2015). We estimated the LOD as 6 μL at *S*/*N* = 3. It is known that the limit of quantification for cholesterol detection, i.e the lowest cholesterol concentration that can be detected experimentally at G/Ti(G)-3DNS/CS/ChOx biosensor, is more accurate with acceptable precision and be different from the LOD reported here. However, the LOD reported in this study can be used for comparison with identically determined LOD values (at *S*/*N* = 3) for other sensors in literature. Table 1 gives the comparison of analytical parameters of some cholesterol biosensors with that of G/Ti(G)-3DNS/CS/ChOx. The comparison revealed that G/Ti(G)-3DNS/CS/ChOx biosensor exhibited relatively high electrochemical sensitivity, a wide linear range concentration and a low LOD for cholesterol detection as compared to other cholesterol sensors (Table 1). Knowing the facts that the desired total plasma cholesterol of an individual is lesser than 5.2 mM (200 mg dL^{-1}) and a higher level of cholesterol concentration beyond which health problem arises being greater than 6.2 mM (240 mg dL^{-1}), the fabricated G/Ti(G)-3DNS/CS/ChOx biosensor may be a promising

Table 1
Comparison of cholesterol sensor analytical performances between G/Ti(G)-3DNS/CS/ChOx biosensor fabricated in this work and other cholesterol sensors.

Electrode materials	LOD/μM	Linear range (mM)	Sensitivity	Ref.
Pt/TMOS sol–gel/ChOx/p(DB)	–	0.06–3.0	0.58 (mA/cm^2 M)	Yao and Takashima (1998)
MWCNTs–ChOxSiO$_2$–chitosan/PB/GCE	1	0.004–0.7	1.55 mA M^{-1}	Tan et al. (2005)
W/ferrocyanide/[ChO/ChEt]	10	0.05–3.0	–	Situmorang et al. (1999)
Nafion/ChOx–Ppy/PB/SAM/Pt	12	0.05–0.3	8.572×10^{-3} (mA/cm^2 M)	Vidal et al. (2004)
ODTA/PB/ChOx Langmuir–Blodgett film	–	0.2–1.2	1.6 (mA/cm^2 M)	Ohnuki et al. (2009)
ChOx/nano-ZnO/ITO	13	0.13–10.4	2.27 (μA/cm^2 mM)	Solanki et al. (2009)
ChOx–ChE/AuNPs/PTH/GCE	0.6	0.002–1.0	2.5 (μA/cm^2 mM)	Huang et al. (2011)
ChOx/AgNPs/GCE	180	0.28–3.3	0.70 (μA/cm^2 mM)	Li et al. (2010)
ChOx/PVF$^+$ClO^{4-}/Pt	–	0.1–0.5	0.14 (μA/cm^2 mM)	Ozer et al. (2007)
G/Ti(G)-3DNS/CS/ChOx	6	0.05–8.0	3.82 (μA/cm^2 mM)	This work

kit for the clinical diagnostics of cholesterol.

3.7. PEC sensing of cholesterol at G/Ti(G)-3DNS/CS/ChOx biosensor (in oxygen containing solution)

The PEC biosensing capability of the G/Ti(G)-3DNS/CS/ChOx biosensor was investigated by the photocurrent measurements in a three electrode PEC cell (in oxygen containing solution). The biocatalytic process of ChOx towards cholesterol is different from that in oxygen free solution (Eqs. (3 and 4)) (Zhu et al., 2013; Li et al., 2015b). In the presence of oxygen, cholesterol is oxidized by ChOx (FAD) to cholest-4-en-3one (Eq. (3)) and the resultant ChOx ($FADH_2$) predominantly involves in the reduction of oxygen to form H_2O_2 (Eq. (5)).

$$ChOx(FADH_2) + O_2 \rightarrow ChOx(FAD) + H_2O_2 \quad (5)$$

The occurrence of reduction of O_2 (Eq. (5)) competitively hinders the DET reaction of ChOx (Eq. (4)). As a result, the electrochemical detection of cholesterol was hindered due to the probable absence of DET. However, the detection of cholesterol concentration by PEC becomes possible under light irradiation. Upon light irradiation, the G/Ti(G)-3DNS/CS/ChOx electrode absorbed the photons and generated the h^+-electron pairs (Eq. (6)).

$$G/Ti(G) - 3DNS\ /CS/ChOx \xrightarrow{h\vartheta} G/Ti(G) - 3DNS\ (h^+) + e^-(\text{photogenerated}) \quad (6)$$

The photogenerated e^- s can be annihilated through participation in H_2O_2 decomposition (Eq. (7)).

$$H_2O_2 + 2H^+ + 2e^-(\text{photogenerated}) \rightarrow 2H_2O \quad (7)$$

Hence, monitoring of photocurrent can be utilized for correlating the cholesterol concentration as an alternate to electrochemical cholesterol sensing. Infect, we achieved cholesterol detection by following photocurrent at −0.05 V through PEC sensing.

Under light irradiation, the photocurrent density of the G/Ti(G)-3DNS/CS/ChOx photoanode was ~1.52 and 1.95 times higher than at G/Ti-3DNS/CS/ChOx and TiO2/CS/ChOx photoanodes, respectively in the presence of 0.5 mM cholesterol (pH 7.0) (Figure not shown). The G/CS/ChOx photoanode exhibited extremely low photocurrent. These results indicated that light irradiation (wavelength=254 nm) significantly improved the sensitivity of G/Ti(G)-3DNS/CS/ChOx. And, the ~2 fold increase in the PEC sensing property of G/Ti(G)-3DNS/CS/ChOx photoanode as compared to pristine TiO_2/CS/ChOx photoanode can be attributed to the following reasons. Due to the existense of the bridged 2D G sheets in G/Ti(G)-3DNS/CS/ChOx, the photogenerated electrons on the conduction band (CB) of TiO_2 NWs transfer to G sheets and cause efficient h^+-electron separation (Xiang et al., 2011; Yang et al., 2010). The G sheets with their excellent electrical conductivity and electron accepting property served as the electron acceptor of the photoexcited electrons (Zhang et al., 2010). Fig. 4B shows the time-dependent "on–off" PEC photocurrent–time (*j*–*t*) responses of the G/Ti(G)-3DNS/CS/ChOx recorded in the presence of 2 mM cholesterol (pH 7.0) at the applied potential of −0.05 V (Fig. 4B). The photocurrent measured in the "turned-on" state (red line) is ~36% higher than in "turned-off", dark current (black line) (Fig. 4B). The photocurrent was stable on several repetitive on–off cycles. These results confirmed that PEC sensing characteristics of G/Ti(G)-3DNS/CS/ChOx photoanode are highly reproducible under measured conditions.

We proposed a mechanism for PEC sensing of cholesterol. The sensing mechanism is mainly based on the generation of photoelectrons (Eq. (6)) coupled with biocatalytic reactions between ChOx and cholesterol leading to the formation of H_2O_2 (Eqs. (3 and 5)). The photogenerated electrons are transferred to G sheets, embedded in G/Ti(G)-3DNS/CS/ChOx 3DNS, whereas the h^+s moved to the electrode interface (Tang et al., 2014). The photogenerated electrons tend to be migrated to G due to the higher Schottly barriers, lower electrical resistivity and larger surface area at the G/TiO_2 interfaces. In the process of avoiding charging effects, the electrons were leaked way from G sheet and transferred to the H_2O_2, generated by the biocatalytic reactions involving ChOx and cholesterol (Eqs. (3 and 5)). As a consequence, a suppression of photocurrents could be resulted. It has been reported that H_2O_2 can be photodecomposed by TiO_2 under light irradiation to produce hydroxyl radicals and H_2O (Legrini et al. 1993; Kumar and Devi 2011; Chen et al. 2012). Thus, the photocurrent suppression was correlated to the concentration of H_2O_2 and in turn to the concentration of cholesterol.

To validate the proposed mechanism, we carried out cholesterol sensing PEC experiments at G/Ti(G)-3DNS/CS (i) in the absence of ChOx and (ii) with increasing concentration of cholesterol. The photocurrent responses of G/Ti(G)-3DNS/CS/ChOx was much lower than the photocurrent at G/Ti(G)-3DNS/CS (without ChOx), which indicated that ChOx also participated in the PEC process. Further, we recorded the amperometric current responses at the "turn-on" conditions for successive addition of cholesterol at G/Ti(G)-3DNS/CS/ChOx photoanode by keeping an applied potential of −0.05 V in 0.1 M PBS (Fig. 4C). For each addition of cholesterol solution, the photocurrent decreased steadily (Fig. 4C). The photocurrent reached a steady value within 2 s before next addition of cholesterol. The photoelectrochemical amperometric results (Fig. 4C) clearly revealed that H_2O_2 indirectly generated by cholesterol through series of reactions (Eqs. (4–7)), caused suppression of the photocurrents. The significant features of our PEC sensing are the short response time (2 s) and good selectivity. Generally, TiO_2 based photocatalysis is non-selective (Kumazawa et al., 2003; Xu et al., 2014; Malekshoar et al., 2014). Hence, TiO_2 based PEC sensing experiments are difficult to design. However, in this work, we utilized the TiO_2 photocatalyst based PEC for cholesterol sensing by exploiting the photo and biocatalytic reactions (Eqs. (3 and 5–7)) and and monitoring the photocurrent at a far negative potential (−0.05 V to achieve excellent selectivity towards cholesterol. Fig. 4C (inset) shows the linear calibration plot for the concentration vs photocurrent. From the calibration plot (Fig. 4C (inset)), it is known that the photocurrent charges were linear upto 5 mM of cholesterol with a high sensitivity of 2.11 μA/cm^2 mM. The LOD of cholesterol through PEC sensing was calculated to be 10 μM (*S*/*N*=3).

3.8. Selectivity, reproducibility and stability of G/Ti(G)-3DNS/CS/ChOx biosensor

The G/Ti(G)-3DNS/CS/ChOx biosensor exhibited excellent selectivity, reproducibility and stability. The details are presented in SI-13.

3.9. Real sample analysis

To evaluate the ability of the G/Ti(G)-3DNS/CS/ChOx biosensor toward real sample analysis, the biosensor was applied to the determination of cholesterol in human blood serum samples. There was no pre-treatment for serum sample other than dilution of the samples. The serum sample (with a cholesterol concentration of 2 mM) was added with 2, 4, and 6 mM of cholesterol from standard solution in PBS and response currents were measured. The concentrations of cholesterol were determined three times and the average values are presented in SI-14 The recovery values

were in the range from 98.25% to 101.76% with relative standard deviations from 1.8% to 3.4%, respectively. The results demonstrated the reliability of G/Ti(G)-3DNS/CS/ChOx biosensor for cholesterol determination in real samples.

4. Conclusions

In conclusion, we have prepared a novel G/Ti(G)-3DNS/CS nanocomposite material, which combined the excellent photocatalytic properties of TiO_2 nanostructures, biocompatibility of CS and electron transport properties and larger surface area of G. The G/Ti(G)-3DNS/CS facilitated the DET between the active centers of ChOx and modified electrode and hence favored the fabrication of DET based electrochemical-PEC dual mode biosensor for the detection of cholesterol. The electrochemical detection of cholesterol was based on DET of ChOx and had wide linear concentration range, high sensitivity and stability. The PEC sensing of cholesterol involved the insitu generated electron acceptor (H_2O_2) via the biocatalytic reaction between ChOx and cholesterol. The highest photocurrent response was achieved for G/Ti(G)-3DNS/CS/ChOx biosensor as compared to the PEC biosensors fabricated with the exclusion of G and/or ChOx, which suggested that the PEC sensing enhancement originated from the improved charge separation at the interface between TiO_2 and G as well through the biocatalytic reaction involving ChOx and cholesterol. The PEC sensing mode offered high selectivity as the photocurrents were monitored at a low applied potential (-0.05 V) The investigated electrochemical-PEC biosensor could be used as a model for future studies toward designing new multiple mode biosensors using other semiconductors-carbon nanostructure based nanocomposites.

Acknowledgments

This work was supported by the Priority Research Centres Program through a National Research Foundation of Korea (NRF) grant funded by the Ministry of Education, Science and Technology (2009-0093819) and a funded research project (NRF-2014R1A1A4A03004026).

Appendix A. Supplementary material

Supplementary data associated with this article can be found in the online version at http://dx.doi.org/10.1016/j.bios.2015.11.042.

References

Arya, S.K., Datta, M., Malhotra, B.D., 2008. Biosens. Bioelectron. 23, 1083–1100.
Bard, A.J., Faulkner, L.R., 2001. Electrochem. Methods 1, 148–207.
Cai, C., Chen, J., 2004. Anal. Biochem. 332, 75–83.
Chen, D., Zhang, H., Liu, Y., Li, J., 2013. Energy. Environ. Sci. 6, 1362–1387.
Chen, H., Nanayakkara, C.E., Grassian, V.H., 2012. Chem. Rev. 112, 5919–5948.
Chong, K.T., Su, X., Lee, E.J.D., O'Shea, S.J., 2002. Langmuir 18, 9932–9936.
Devadoss, A., Sudhagar, P., Terashima, C., Nakata, K., Fujishima, A., 2015. J. Photochem. Photobiol. C 24, 43–63.
Gholivand, M.B., Khodadadian, M., 2014. Biosens. Bioelectron 53, 472–478.
Gopalan, A.I., Lee, K.P., Ragupathy, D., 2009. Biosens. Bioelectron. 24, 2211–2217.
Huang, Q., An, Y., Tang, L., Jiang, X., Chen, H., Bi, W., Wang, Z., Zhang, W., 2011. Anal. Chim. Acta 707, 135–141.
Han, S., Jiang, J., Huang, Y., Tang, Y., Cao, J., Wu, D., Feng, X., 2015a. Phys. Chem. Chem. Phys. 17, 1580–1584.
Han, Q., Wang, K., Xu, L., Yan, X., Zhang, K., Chen, X., Wang, Q., Zhang, L., Pei, R., 2015b. Analyst. 140, 4143–4147.
Hu, Y., Xue, Z., He, H., Ai, R., Liu, X., Lu, X., 2013. Biosens. Bioelectron. 47, 45–49.
Komathi, S., Gopalan, A.I., Kim, S.K., Anand, G.S., Lee, K.P., 2013. Electrochim. Acta 92, 71–78.
Kumar, S.G., Devi, L.G., 2011. J. Phys. Chem. A 115, 13211–13241.
Kumazawa, H., Inoue, M., Kasuya, T., 2003. Ind. Eng. Chem. Res. 42, 3237–3244.
Lee, H.G., Sai-Anand, G., Komathi, S., Gopalan, A.I., Kang, S.W., Lee, K.P., 2015a. J. Hazard. Mater. 283, 400–409.
Lee, H.G., Gopalan, A.I., Sai-Anand, G., Lee, B.C., Kang, S.W., Lee, K.P., 2015b. Mater. Chem. Phys. 154, 125–136.
Lee, J.S., You, K.H., Park, C.B., 2012. Adv. Mater. 24, 1084–1088.
Legrini, O., Oliveros, E., Braun, A.M., 1993. Chem. Rev. 93, 671–698.
Li, H., Wang, X., Zhang, L., Hou, B., 2015a. Nanotech 26, 155704.
Li, Y., Bai, H., Liu, Q., Bao, J., Han, M., Dai, Z., 2010. Biosens. Bioelectron 25, 2356–2360.
Li, Z., Xie, C., Wang, J., Meng, A., Zhang, F., 2015b. Sens. Actuators B 208, 505–511.
Lin, K.C., Jian, X.C., Chen, S.M., 2011. Int. J. Electrochem. Sci. 6, 2264–2283.
Liu, B., Aydil, E.S., 2009. J. Am. Chem. Soc. 131, 3985–3990.
Ma, Y., Zhang, J., Tian, B., Chen, F., Wang, L., 2010. J. Hazard. Mater. 182, 386–393.
Malekshoar, G., Pal, K., He, Q., Yu, A., Ray, A.K., 2014. Ind. Eng. Chem. Res. 53, 18824–18832.
Manesh, K.M., Santhosh, P., Uthayakumar, S., Gopalan, A.I., Lee, K.P., 2010. Biosens. Bioelectron. 25, 1579–1586.
Manjunatha, R., Nagaraju, D.H., Suresh, G.S., Melo, J.S., D'Souza, S.F., Venkatesha, T. V., 2011. J. Electroanal. Chem. 651, 24–29.
Manjunatha, R., Suresh, G.S., Melo, J.S., D'Souza, S.F., Venkatesha, T.V., 2012. Talanta 99, 302–309.
Ohnuki, H., Honjo, R., Endo, H., Imakubo, T., Izumi, M., 2009. Thin Solid Films. 518, 596–599.
Ozer, B. C., Ozyoruk, H., Çelebi, S. S., Yıldız, A., 2007. Enzyme Microb. Technol. 40, 262-265.
Rathi, S., Lee, I., Lim, D., Wang, J., Ochiai, Y., Aoki, N., Watanabe, K., Taniguchi, T., Lee, G.H., Yu, Y., Kim, J., Kim, G. H., P., 2015. Nano Lett. 15, 5017–5024.
Ruecha, N., Rangkupan, R., Rodthongkum, N., Chailapakul., O., 2014. Biosens. Bioelectron. 52, 13–19.
Ruecha, N., Siangproh, W., Chailapakul, O., 2011. Talanta 84, 1323–1328.
Sai-Anand, G., Gopalan, A.I., Kang, S.W., Lee, K.P., 2013. IEEE Electron Device Lett. 34, 1065–1067.
Sekretaryova, A.N., Beni, V., Eriksson, M., Karyakin, A.A., Turner, A.P.F., Vagin, M., 2014. Anal. Chem. 86, 9540–9547.
Sharma, R., Sinha, R.K., Agrawal, V.V., 2015. RSC Adv. 5, 41786–41794.
Sheng, M., Gao, Y., Sun, J., Gao, F., 2014. Biosens. Bioelectron. 58, 351–358.
Siswana, M.P., Ozoemena, K.I., Nyokong, T., 2006. Electrochim. Acta 52, 114–122.
Situmorang, M., Alexander, P. W., Hibbert, D. B., 1999. Talanta. 49, 639-649.
Solanki, P. R., Kaushik, A., Ansari, A. A., Malhotra, B. D., 2009. Appl. Phys. Lett. 94, 143901.
Stafiniak, A., Boratynski, B., Baranowska-Korczyc, A., Szyszka, A., Ramiączek-Krasowska, M., Prazmowska, J., Fronc, K., Elbaum, D., Paszkiewicz, R., Tlaczala, M., 2011. Sens. Actuators B 160, 1413–1418.
Suginta, W., Khunkaewla, P., Schulte, A., 2013. Chem. Rev. 113, 5458–5479.
Tan, X., Li, M., Cai, P., Luo, L., Zou, X., 2005. Anal. Biochem. 337, 111–120.
Tang, J., Wang, Y., Wang, Y., Li, J., Kong, B., Jiang, M., Zheng, G., 2014. J. Mater. Chem. A 2, 15752–15757.
Tong, P., Shao, Y., Chen, J., He, Y., Zhang, L., 2015. Anal. Methods 7, 2993–2999.
Ueda, A., Kato, D., Kurita, R., Kamata, T., Inokuchi, H., Umemura, S., Niwa, O., 2011. J. Am. Chem. Soc. 133, 4840–4846.
Unnikrishnan, B., Palanisamy, S., Chen, S.M., 2013. Biosens. Bioelectron. 39, 70–75.
Van Gough, D., Lambert, T.N., Wheeler, D.R., Rodriguez, M.A., Brumbach, M.T., Allendorf, M.D., Spoerke, E.D., 2014. ACS Appl. Mater. Interfaces 6, 1509–1514.
Vidal, J. C., Espuelas, J., Garcia-Ruiz, E., Castillo, J. R., 2004. Talanta 64, 655–664.
Wu, X., Yin, S., Dong, Q., Guo, C., Li, H., Kimura, T., Sato, T., 2013. Appl. Catal. B Environ. 142, 450–457.
Xiang, Q., Yu, J., Jaroniec, M., 2011. Nanoscale 3, 3670–3678.
Xu, C., Rangaiah, G.P., Zhao, X.S., 2014. Ind. Eng. Chem. Res. 53, 14641–14649.
Yang, N., Zhai, J., Wang, D., Chen, Y., Jiang, L., 2010. Acs Nano 4, 887–894.
Yao, T., Takashima, K., 1998. Biosens. Bioelectron. 13, 67–73.
Zang, Y., Lei, J., Zhang, L., Ju, H., 2014. Anal. Chem. 86, 12362–12368.
Zhang, H., Lv, X., Li, Y., Wang, Y., Li, J., 2010. ACS Nano 4, 380–386.
Zhu, L., Xu, L., Tan, L., Tan, H., Yang, S., Yao, S., 2013. Talanta 106, 192–199.
Zhuang, Z., Su, X., Yuan, H., Sun, Q., Xiao, D., Choi, M.M., 2008. Analyst 133, 126–132.